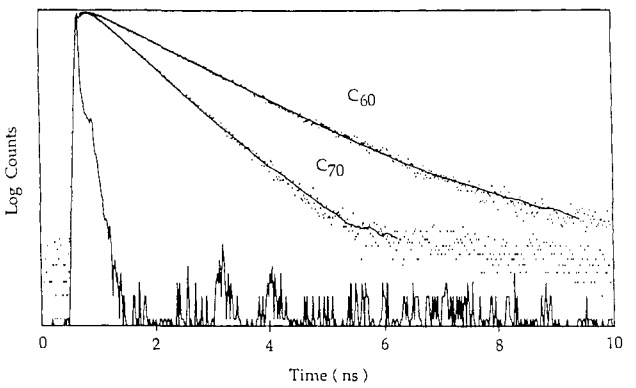

Figure 2. Log-linear plot of fluorescence decay curves for C_{60} and C_{70} in toluene at room temperature. Shown in the short-time region is the instrument response function for our time-correlated single photon counting scheme.

1400 ± 100 cm^{-1} spacings, which most likely was a manifestation of the 1469-cm^{-1} mode.

The splitting between the two major peaks in our C_{60} spectrum (Figure 1) is determined to be about 490 cm^{-1}, which is comparable to the one for the solid sample at 5 K.[6] We believe that this corresponds to the energy of a vibrational quantum for the other totally symmetric (A_g), Raman active breathing mode in the ground state,[14] 496 cm^{-1}. In fact, the emission spectra from 20 K film also seem to reveal the same feature, although it is not explicitly mentioned (upper spectrum of Figure 3 of ref 5).

The fluorescence spectrum of C_{70} shows a maximum at significantly shorter wavelengths near 15 000 cm^{-1}. Here again, polycrystalline solid at 5 K gives a spectrum similar to that of our room temperature sample, the only difference being the relative peak heights.[6] The recently reported emission spectrum of C_{70} at 77 K shows a much better resolved fine structure,[7] but our room temperature solution spectrum clearly gives a rough envelope of it. It is estimated that when calibrated against the same optical density, the fluorescence intensity of C_{60} at the peak is about 5 times weaker than that of C_{70}. The fluorescence quantum yield for the latter has been estimated to be about 8.5×10^{-4} by comparison with the tetracene fluorescence at 540 nm.[7] We thus expect the fluorescence quantum yield of C_{60} in room temperature solution to be about 2×10^{-4}, which is in good agreement with a conservative estimate for the lower bound of 10^{-4}.[13]

Time-correlated single photon counting (TCSPC) detection was carried out to determine the lifetimes of the singlet states of C_{60} and C_{70} in solution. The laser source consists of a CW mode-locked Nd:YAG laser and a cavity-dumped dual-jet dye laser. The dye laser pulses with a pulse energy of 10–18 nJ at 570–605 nm, and a repetition rate of 3.8 MHz was monitored by a real-time autocorrelator. The pulse width was measured to be 1 ps. With the use of a microchannel plate photomultiplier tube (Hamamatsu Model R2809), it was possible to obtain an instrument response function as short as 25 ps. To eliminate rotational contribution to the fluorescence lifetime, the fluorescence emission from the sample was detected at the magic angle with respect to the excitation polarization, and a polarization scrambler was put in front of the monochromator. Toluene and benzene of HPLC grade were used as solvents. To check the possibility of impurity fluorescence, these pure solvents alone (without C_{60} or C_{70}) were excited at 587 nm and monitored over 600–850 nm. No fluorescence was observed in this wavelength region. All the fullerene solutions were degassed by a freeze–pump–thaw cycle three times before each use.

The fluorescence decay curves for both C_{60} and C_{70} in toluene are shown in the semilog plot of Figure 2. It is clearly seen that each shows a single exponential decay. By a deconvolution technique with nonlinear curve fitting, the lifetimes are determined to be 1.17 ± 0.02 ns for C_{60} and 0.66 ± 0.02 ns for C_{70}. The calculated curves based on these lifetimes are also shown in the figure. The fluorescence lifetimes of undegassed samples were measured as well and found to be shorter by 5–6% for both C_{60} and C_{70}. Lifetimes were also measured as a function of concentration. There was no difference in lifetimes over the concentration range 1×10^{-4} to 2×10^{-3} M within the error limit of 4%. The lifetime was also measured as a function of laser power and turned out to be independent of excitation intensity. The lifetimes of C_{60} and C_{70} in benzene solution were essentially identical with those in toluene solution. Our values of the lifetimes for S_1 states of C_{60} and C_{70} by the TCSPC technique confirm those of some of the earlier measurements by a less direct method of transient absorption, which reported lifetimes of 1.2 ns for C_{60}[8] and 0.67 ns for C_{70}.[10]

These results are in fact consistent with the weak fluorescence intensity observed (in our experiment), as first pointed out by Hochstrasser and co-workers.[9] If only the shoulder around 630 nm of the absorption spectrum is assigned to the $S_0 \rightarrow S_1$ transition, the radiative lifetime is estimated to be $2.9g_u$ μs, where g_u is the degeneracy of the emitting state, usually taken as 3. On the other hand, if the same transition gives rise to the entire visible absorption spectrum, a lower limit of the radiative lifetime is estimated to be $0.24g_u$ μs. Thus our measured excited-state lifetime of 1.17 ns for C_{60} yields the fluorescence quantum yield of 1.17 ns/$2.9g_u$ μs = $4 \times 10^{-4}/g_u$, with a possible upper limit of ca. $5 \times 10^{-3}/g_u$. Our previously estimated fluorescence quantum yield of ca. 2×10^{-4} not only is in good agreement with these results but also suggests that only a relatively narrow band of absorption is possibly due the $S_0 \rightarrow S_1$ transition.

Acknowledgment. This work was supported by the SNU Daewoo Research Fund, the University–KRISS joint research program, and KOSEF funds to D.K. and S.K.K. through the Center for Molecular Science. We thank Mr. O. K. Song for recording the fluorescence spectra, Mr. W. Kim for help in the design stage of the contact-arc machine, and Mr. S. M. Jin for the production and separation of fullerenes.

Supplementary Material Available: Mass spectra and mass spectral data for C_{60} and C_{70} (6 pages). Ordering information is given on any current masthead page.

Equivalent Li···O and H···O Electronic Effects in the Lithium Enolate of 1,3-Cyclohexanedione

Margaret C. Etter* and Gandara Ranawake

Chemistry Department
University of Minnesota
Minneapolis, Minnesota 55455

Received October 29, 1991

The question of the structural and electronic equivalence of lithium and hydrogen has been addressed both theoretically and experimentally.[1] The current view is that lithium structures are more complex than their H-bonded analogs due to the multiple coordination sites available for lithium. In addition, interactions between Li and electron-rich atoms like oxygen and nitrogen are stronger than the similar interactions involving H. We report here two unexpected structures containing both Li···O and H···O interactions where lithium and hydrogen have nearly identical coordinating abilities to the two conjugated oxygen atoms of 1,3-cyclohexanedione (CHD) lithium enolate (Li-CHD).

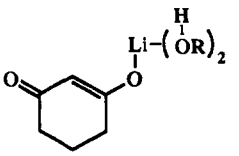

I. R = $-CH_3$

II. R = $-CH_2CF_3$

* Alfred P. Sloan Fellow, 1989–1991.

(1) Sannigrahi, A. B.; Kar, T.; Guha Niyogi, B.; Hobza, P.; Schleyer, P. v. R. *Chem. Rev.* **1990**, *90*, 1061–1076 and references therein.

0002-7863/92/1514-4430$03.00/0

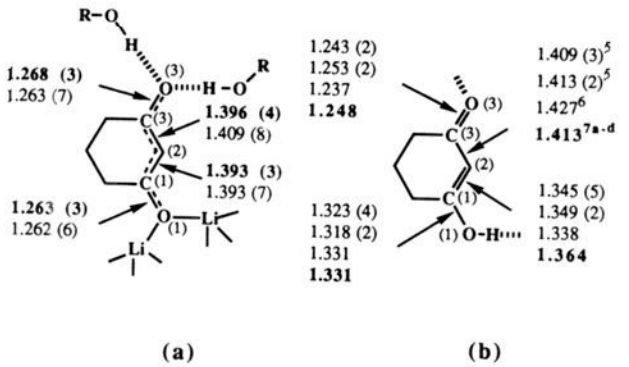

Figure 1. (a) Alcohol-solvated lithium enolates. The bond distances (Å) and angles (deg) are from the crystal structures of the methanol (bold type), I, and 2,2,2-trifluoroethanol, II, solvates. Selected intramolecular bond angles are as follows: O(1)–C(1)–C(2) = **123.2 (2)**, 123.4 (5); O(3)–C(3)–C(2) = **123.3 (2)**, 122.6 (5). (b) The first three bond distances (Å) are those from three different known crystal structures of plain CHD,[5,6] and the last distance (bold type) is the average of three known crystal structures of its simple derivatives.[7a–d] (Although the six structures represented by this figure contain varying conformations, the particular one illustrated here is the syn-anti conformation.)

Clear, well-shaped crystals of enolates I and II were readily obtained by slow evaporation of a methanol or 2,2,2-trifluoroethanol solution of Li-CHD[2] at room temperature, under nitrogen. They were shown to be the bis-solvated lithium enolates[3] by solution ^{1}H NMR. The proposed structures of I and II were confirmed by single-crystal low-temperature X-ray diffraction.[4]

The crystal structures of I and II show that two alcohol molecules are associated with O(3) by strong H-bonds, while two Li atoms are associated with O(1) of Li-CHD, Figure 1a. In both structures, the π system of Li-CHD is completely delocalized with equal C–O bond lengths and central C–C bond lengths. Such complete delocalization is not seen in CHD structures, where the molecules are associated only by hydrogen bonds, Figure 1b.[5]

The delocalization of the π systems of I and II is also apparent from analysis of the solid-state ^{13}C CP/MAS NMR spectral data. While plain CHD shows two peaks at 186.9 and 203.9 ppm for the enol carbon and the carbonyl carbon, respectively,[5] I and II show only one peak, at 198.2 ppm (I) and 197.3 ppm (II),[8] indicating that the C–O carbons have nearly identical electronic environments in the solid state.[2]

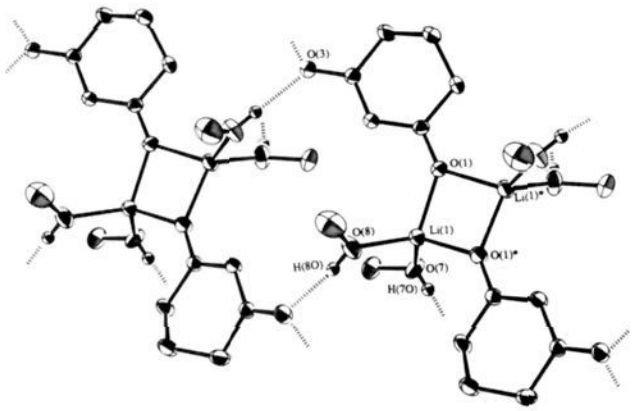

Figure 2. ORTEP drawing of I showing the aggregate pattern resulting from Li···O and O···H interactions (hydrogen atoms have been removed for clarity except for the methanol OH hydrogen). A nearly identical pattern is also found for II (shown in the supplementary material). Selected intermolecular bond distances (Å), angles (deg), and torsion angles (deg) are as follows: Li···O(1) = 1.935 (3); Li···O(1)* = 1.945 (5); Li···O(8) = 1.913 (5); Li···O(7) = 1.919 (5); O(3)···O(7) = 2.669 (4); O(3)···H(7O)–O(7) = 171.68 (2); O(3)···O(8) = 2.656 (2), O(3)···H(8O)–O(8) = 173.70 (2); Li(1)–O(1)–C(1)–C(2) = 10.7 (4), Li(1)*–O(1)–C(1)–C(2) = –171.7 (3), H(8O)–O(3)–C(3)–C(2) = –7.0 (2), H(7O)–O(3)–C(3)–C(2) = 145.0 (1).

The lithium atoms in I and II form four-membered rings with the two enolate oxygens O(1) and are solvated by two alcohol oxygens each. These dimeric enolate units have 2-fold symmetry in I, as shown in Figure 2, and inversion symmetry in II. Similar dimeric aggregate structures have frequently been observed in other lithium enolate structures.[9]

Both oxygens of I and II have intermolecular contacts (either H or Li) at all available syn and anti lone-pair positions. In the CHD structures, where there is only one coordinating hydrogen atom, there appears to be stereoelectronic selectivity during hydrogen bond formation. Two examples of observed CHD hydrogen bond patterns, anti-anti and syn-anti (specifying the enolic proton orientation first), are shown below for purposes of comparison to the aggregate structures of I and II.

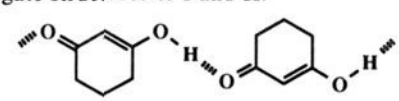

In summary, converting CHD to its lithium enolate causes the π system to delocalize completely in the solid state. Two hydrogen bonds to one Li-CHD oxygen appear to influence the Li-CHD electronic structure to the same extent as the two lithium bonds at the other, conjugated, Li-CHD oxygen.

Acknowledgment. We gratefully acknowledge Professor Doyle Britton, University of Minnesota, for crystallographic assistance and the NSF (CHEM 8821778) for financial support. Helpful discussions with Dr. Daniel Adsmond, University of Minnesota, and Dr. Susan Reutzel, Lilly Research Laboratories, Eli Lilly and

(2) See supplementary material for preparation, characterization, and solid-state NMR data.

(3) The ratio of lithium enolate to alcohol was established by the ratio of the integrated intensities among the methylene hydrogen peaks in Li-CHD and the methyl hydrogen peak in MeOH [δ 1.69 (2 H), 1.95 (4 H), and 3.16 (6 H)] for I and the methylene hydrogen peak in 2,2,2-trifluoroethanol [δ 1.73 (2 H), 1.97 (4 H), and 3.86 (4 H)] for II.

(4) Crystal data for I: $C_8H_{15}O_4Li$, fw = 182.15, monoclinic, $C2$, a = 15.540 (7) Å, b = 8.508 (8) Å, c = 8.927 (4) Å, β = 120.76 (3)°, V = 1014 (2) Å^3, Z = 4, D_{calcd} = 1.19 g/cm^3, λ(Mo Kα) = 0.71069 Å, μ = 0.86 cm^{-1}, F(000) = 392, T = –101 °C, R_w = 0.051, R = 0.039. Crystal data for II: $C_{10}H_{13}O_4LiF_6$, fw = 318.14, triclinic, $P\bar{1}$, a = 8.84 (1) Å, b = 9.03 (1) Å, c = 9.70 (1) Å, α = 99.4 (1)°, β = 92.6 (1)°, γ = 117.33 (9)°, V = 627 (3) Å^3, Z = 2, D_{calcd} = 1.572 g/cm^3, λ(Mo Kα) = 0.71069 Å, μ = 1.60 cm^{-1}, F(000) = 324, T = –101 °C, R_w = 0.082, R = 0.076. See supplementary material for complete crystallographic details.

(5) Etter, M. C.; Urbańczyk-Lipkowska, Z.; Jahn, D. A.; Frye, J. S. *J. Am. Chem. Soc.* **1986**, *108*, 5871–5876.

(6) Katrusiak, A., Adam Mickiewicz University, Poznań, Poland, private communication. A third polymorph of CHD with an alternate syn-anti and anti-syn stereoelectronic pattern (specifying the enolic proton orientation first) was found. Since there are four molecules in the asymmetric unit, only their average bond distances are reported in Figure 1b.

(7) Complete tables of bond lengths for each crystal structure are provided as supplementary material: (a) Low, J. N.; Wilson, C. C. *Acta Crystallogr.* **1983**, *C39*, 1688–1690. (b) Singh, I.; Calvo, C. *Can. J. Chem.* **1975**, *53*, 1046–1050. (c) Semmingsen, D. *Acta Chem. Scand.* **1974**, *B28*, 169–174. (d) Belyaeva, K. F.; Kuklin, V. N.; Smorigo, N. A.; Byushkin, V. N.; Malinovskii, T. L.; Ivin, B. A. *J. Struct. Chem.* **1986**, *27* (*3*), 448–454.

(8) Each spectrum was obtained with 2K data points, zero filled to 8K prior to Fourier transformation, with line broadening set to 5 Hz and with a 10000 Hz spectral window width. Estimated error limits (esd) of solid-state spectra are ±0.5 ppm.

(9) (a) Laube, T.; Dunitz, J. D.; Seebach, D. *Helv. Chim. Acta* **1985**, *68*, 1373–1393. (b) Amstutz, R.; Dunitz, J. D.; Laube, T.; Schweizer, W. B.; Seebach, D. *Chem. Ber.* **1986**, *119*, 434–443. (c) Amstutz, R.; Dunitz, J. D.; Laube, T.; Schweizer, W. B.; Seebach, D. *J. Am. Chem. Soc.* **1985**, *107*, 5403–5409. (d) Bauer, W.; Laube, T.; Seebach, D. *Chem. Ber.* **1985**, *118*, 764–773.

Company, are also appreciated.

Registry No. I, 140925-97-9; II, 140925-99-1.

Supplementary Material Available: Crystallographic details including positional parameters, thermal parameters, intra- and intermolecular bond lengths and bond angles, and unit cell drawings, experimental section for I and II, and listings of bond distances of the third form of CHD and CHD derivatives (26 pages); listing of observed and calculated structure factors for I and II (22 pages). *Ordering information is given on any current* masthead page.

New Approach To Producing Patterned Biomolecular Assemblies

Suresh K. Bhatia,[†] James J. Hickman,[‡] and Frances S. Ligler*[,§]

Geo-Centers, Inc.
Fort Washington, Maryland 20744
Science Applications International Corp.
McLean, Virginia 22102
Center for Bio/Molecular Science and Engineering
Code 6090, Naval Research Laboratory
Washington, D.C. 20375-5000
Received February 3, 1992

A key requirement to the integration of biomolecules into complex structures and materials is the ability to specify the site of immobilization, preferably on a submicron scale.[1] A major difficulty in immobilizing proteins in specific patterns on a surface is not the chemistry required for immobilization but the methodology for preventing proteins from absorbing to unwanted regions. Previous methods for forming protein patterns required lift-off procedures or exposure to denaturants to remove proteins adsorbed in the wrong areas.[2-6] We have created photolithographically patterned surfaces with clearly defined regions of high and low protein adsorptivity by exposing silica surfaces treated with (3-mercaptopropyl)trimethoxysilane (MTS) to UV light through a mask. Upon exposure of an MTS-coated surface to UV light in the presence of oxygen, X-ray photoelectron spectroscopy (XPS) indicates that the thiol terminal is oxidized. The resulting surface is resistant to protein adsorption. Antibodies immobilized in patterns using this method retain their antigen binding capability.

One approach to the creation of a self-assembling three-dimensional structure using biomolecules as building blocks begins with a two-dimensional template which has the ability to direct the construction of subsequent layers. For making patterns of biomolecules, such a template must include areas which resist nonspecific adsorption. To this end, we investigated the extent of protein adsorption on MTS, (3-aminopropyl)trimethoxysilane, [3-[*N*-(2-aminoethyl)amino]propyl]trimethoxysilane, [3-(glycidyloxy)propyl]trimethoxysilane, and (tridecafluoro-1,1,2,2-tetrahydrooctyl)dimethylchlorosilane films before and after deep UV exposure. Glass surfaces coated with silane films were irradiated with a low-pressure Hg(Ar) lamp for 10 min and incubated with ^{125}I-labeled goat immunoglobulin G (IgG). The amounts of radiolabeled protein adsorbed onto the unirradiated and irradiated surfaces were calculated in each case using radioactive counts from the scintillation counter.[7]

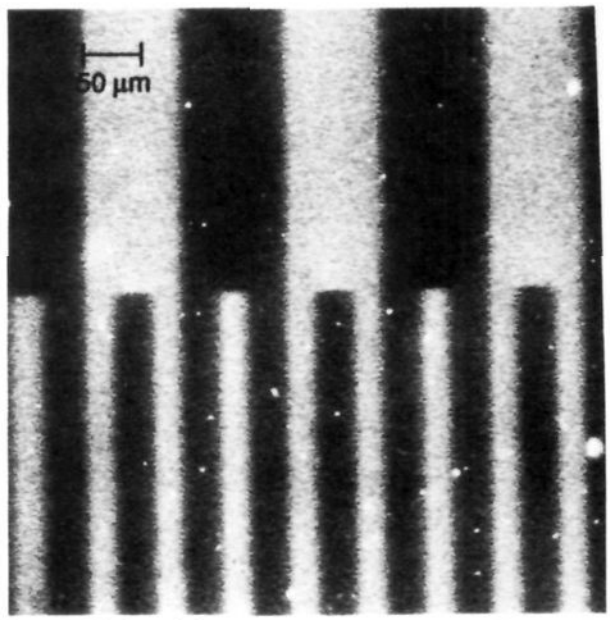

Figure 1. High-resolution pattern of fluorescent protein. Phycoerythrin was covalently immobilized[9] on a patterned thiol silane film and examined using confocal fluorescence microscopy.

With amine, epoxy, and perfluoro silane films, little or no change in the protein adsorption occurred as a function of irradiation. However, the amount of radiolabeled protein adsorbed on MTS dropped from 1.2 ± 0.2 ng/mm^2 to 0.17 ± 0.02 ng/mm^2 following irradiation, corresponding to an 86% reduction compared to the unirradiated surface. In similar experiments, irradiation of an MTS-coated slide reduced adsorption of BSA, a protein well-known for its propensity to adhere to surfaces,[8] by 75% and that of glucose oxidase by 90%. Subsequent treatment of irradiated MTS films with the heterobifunctional cross-linker *N*-[(γ-maleimidobutyryl)oxy]succinimide (GMBS) did not increase the amount of radiolabeled IgG bound to the irradiated surface (0.15 ± 0.02 ng/mm^2). Thus, the thiol groups with which GMBS specifically reacts[9,10] were no longer available after irradiation of the coated surface.

Patterns of covalently attached proteins were produced by placing a high-resolution mask in mechanical contact with an MTS-coated substrate and irradiating the surface with UV light. The irradiated films were then incubated separately with and without GMBS and a fluorescent protein, phycoerythrin.[11] Subsequent visualization using a confocal fluorescence microscope indicated selective attachment of the protein to the unirradiated areas (Figure 1).

Irradiation of an MTS-coated substrate through a low-resolution mask and incubation with GMBS[9] and radiolabeled IgG resulted in selective attachment of the antibody to unirradiated areas visualized by autoradiography. Retention of function following covalent immobilization was also demonstrated by attaching the unlabeled antibody, rabbit anti goat IgG, to a patterned silane film using GMBS. Radiolabeled antigen, goat IgG, was then added. Autoradiographs indicated that antibody immobilized in the regions protected from UV light was still capable of binding

* Author to whom correspondence should be addressed.
[†] Geo-Centers, Inc.
[‡] Science Applications International Corp.
[§] Naval Research Laboratory.

(1) Swalen, J. D.; Allara, D. L.; Andrade, J. D.; Chandross, E. A.; Garoff, S.; Israelachvili, J.; McCarthy, T. J.; Murray, R.; Pease, R. F.; Rabolt, J. F.; Wynne, K. J.; Yu, H. *Langmuir* **1987**, *3*, 932-950.
(2) Lowe, C. R.; Earley, F. G. P. US Patent No. 4,562,157, 1985.
(3) McAlear, J. M.; Wehrung, J. M. US Patents No. 4,103,064, 4,103,073, 1978.
(4) Britland, S.; Perez-Arnaud, E.; Clark, P.; McGinn, B.; Connoly, P.; Moores, G. *Biotechnol. Prog.* **1992**, *8*, 155-160.
(5) Vopel, T.; Ladde, A.; Muller, H. *Anal. Chim. Acta* **1991**, *251*, 117-120.
(6) Hanazato, Y.; Nakako, M.; Maeda, M.; Shiono, S. *Anal. Chim. Acta* **1987**, *193*, 87-96.
(7) Two reference samples containing known amounts of radiolabeled protein were prepared and radioactive counts obtained on a scintillation counter. Thus the counts obtained with immobilized samples were quantitated using the numbers from reference samples.
(8) Lee, S. H.; Ruckenstein, E. *J. Colloid Interface Sci.* **1988**, *125*, 365-379.
(9) Bhatia, S. K.; Shriver-Lake, L. C.; Prior, K. J.; Georger, J. H.; Calvert, J. M.; Bredehorst, R.; Ligler, F. S. *Anal. Biochem.* **1989**, *178*, 408-413.
(10) Ligler, F. S.; Calvert, J. M.; Georger, J. H.; Shriver-Lake, L. C.; Bhatia, S. K.; Bredehorst, R. US Patent No. 5,077,210, 1991.
(11) Oi, V. T.; Glazer, A. N.; Stryer, L. *J. Cell Biol.* **1982**, *93*, 981-986.

0002-7863/92/1514-4432$03.00/0